SUPPLEMENTAL MATERIAL

This PDF includes:

I) Detailed description of the materials and methods

II) Legends for Supplementary Figures I - IX

III) Legends for Videos I - VI

IV) Supplementary Figures I - IX

V) Schematic of the mapping and connection for electrode array with the DAQ system

Other supplementary materials for this manuscript include the following:

Videos I - VI

Materials and Methods

The data, methods, and study materials will be made available for other researchers upon request for the purposes of developing new methods of analysis, reproducing the results or replicating the procedure. Detailed description of the materials and methods are available in the supplementary materials.

Study design

All studies (n=30) using de-identified human heart tissue were approved by the Institutional Review Board (Office of Human Research) at the George Washington University and University of California Los Angeles. In total for this study, we procured 29 de-identified donor human hearts from Washington Regional Transplant Community (WRTC). One additional donor heart was procured through the UCLA Cardiac Arrhythmia Center in Los Angeles, California. All hearts were arrested using ice-cold cardioplegic solution in the operating room and transported to the laboratory for dissection and subsequent electrophysiology, transcriptome, and immunostaining studies. A complete list of hearts with available clinical information is shown in Supplementary Figure I.

This was a prospective, non-randomized study, and the investigators were not blinded to the data. Three donor hearts (Group 0) were used to conduct exploratory research including development of study protocol and the techniques for RVOT wedge dissection, cannulation, and perfusion. Donor hearts were grouped to investigate the effects of cholinergic and adrenergic modulation using optical mapping. Group 1 (n=7; male=3, female=4) donor hearts

were used to study the effects of cholinergic and adrenergic stimulation in isolation. Group 2 (n=6; male=3, female=3) was used to evaluate the effects of cholinergic stimulation in donor hearts already subjected to adrenergic stimulation. Since fresh tissue samples could not be extracted from Groups 1 and 2, additional Group 3 donor hearts were used to collect tissue for RNA sequencing (n=10; male=5, female=5) and immunostaining (n=4; male=1, female=3) studies. Group 3 was not subjected to functional studies in order to avoid likely changes in transcriptome caused by in vitro perfusion. While optical mapping was the primary modality for functional studies, we also conducted simultaneous optical and electrical mapping in 3 donor hearts to validate optical mapping with a clinically relevant electrical mapping.

All data and software used for functional, transcriptomic, and immunostaining studies will be made available through the online repository at the George Washington University.

Experimental preparation and study protocol

Dual sided (epicardial and endocardial) optical and electrical mapping experiments were conducted in RVOT preparations from donor human hearts (Figure 1A). To prepare the RVOT wedge, the aorta and the pulmonary artery were dissected open to expose and isolate the right and left coronary arteries for cannulation. Most of the atria, the left ventricle (LV), and the posterior right ventricle (RV) were removed to expose the anterior RV and the RVOT surface area. The remaining vessel branches were tied off. The RVOT preparation was stretched across a frame and secured to pull it flat (Figure 1B). Methylene blue was applied to ensure adequate perfusion and the preparation was transferred to oxygenated Tyrode's solution maintained at 37 °C, with a perfusion pressure of 60-80 mmHg. The tissue was suspended vertically in a bath

to allow optical access to both the endocardial and epicardial surface. The preparation was washed with 2L of Tyrode's solution to remove excess transplant solution and restore basal electrophysiology. Tissue was immobilized by blebbistatin (10-15 μM) to suppress motion artifacts in optical recordings, without adverse electrophysiological effects. Di-4-ANBDQBS was used to map transmembrane potential as previously described. Pseudo-ECGs were recorded with Ag/AgCl electrodes clipped to the endocardial surface. A platinum tipped bipolar electrode was used for endocardial pacing.

Tissue was paced from the endocardium using a dynamic restitution protocol (S1S1) to assess rate dependence of action potential duration (APD). Briefly, the S1S1 protocol entails pacing the tissue for at least 60 beats at constant cycle length (S1S1), and then repeating the process by progressively shortening the S1-S1 intervals. This restitution protocol was executed after each treatment. Pacing current was adjusted to twice the diastolic pacing threshold starting at pacing cycle length (CL) of 2000 ms (heart rate at 30 BPM) and progressively decreased to functional refractory period (FRP). For Group 1, the tissue was treated with acetylcholine (100 μM) and the restitution protocol repeated. Following that, acetylcholine was washed out, and the tissue was treated with isoproterenol (100 nM). The restitution protocol was repeated until arrhythmia was induced (Figure 1C). For Group 2, the tissue was first treated with isoproterenol (100 nM) and the restitution protocol repeated. The tissue was then subjected to acetylcholine (100 μM) treatment, while still under the influence of sympathetic stimulation (no washout of isoproterenol). In case the S1S1 restitution protocol alone was unable to induce arrhythmia, burst pacing (50Hz) in combination with pinacidil (50 μM) was used for arrhythmia induction.

Only in two cases (D3 and D10) we were unable to induce arrhythmia. All arrhythmias induced were sustained and lasted for at least 15 minutes.

Optical Cardiac Mapping

Optical action potentials were mapped from ~7cm x 7cm (spatial resolution 700μM) field of view from the two surfaces (epicardium and endocardium) using two MiCAM05 (SciMedia, CA) CMOS cameras (100 x 100 pixels). The field of views for both cameras were centered and spatially aligned for dual-sided mapping. Four-second or eight-second recordings were captured at 1KHz sampling frequency. Premature ventricular contractions (PVCs) were tracked from the pseudo-ECGs recorded during the experiment using Lab Chart (ADInstruments, CO).

All optical signals were processed in MATLAB version 2020a. Briefly, each pixel was spatially filtered with a 3x3 uniform average bin, the temporal sequences were low pass filtered using a Finite Impulse Response (FIR) filter with a cutoff frequency of 100Hz, drift in the baseline was removed with a polynomial fit subtraction, and the magnitude of the fluorescent change was normalized. Activation times were determined by calculating the time of dF/dt_{max}, which corresponds to the steepest segment of the optical action potential upstroke (Supplementary Figure IIA). Action potential duration was calculated at 80% repolarization (APD80).

To measure the extent of spatial organization during ventricular tachyarrhythmia, indices including dominant frequency (DF), regularity index (RI), and organization index (OI) were evaluated for each pixel. DF was defined as the frequency band with maximal power on a periodogram calculated with a Fast-Fourier transform (resolution 0.25Hz). RI was defined as the

ratio of power within a 1.5Hz band centered on the DF and the total power spectrum from 3 to 20 Hz. OI was defined as the ratio of the spectral power in a 1.5Hz band centered on the DF including the areas under harmonic frequencies and the total power spectrum from 3 to 20Hz. Single parameter spatial maps were aligned using MATLAB's intensity-based image registration to account for any small translation or scaling differences in camera orientation between fields of view before statistical comparisons.

To evaluate the complexity of arrhythmias including wavefront dynamics, phase singularity dynamics and endo/epi dissociation dynamics, the optical signals were transformed into the phase domain using the Hilbert Transform (Supplementary Figure IIB).

Wavefronts were defined as the isophase lines along $\varphi=\pi/2$. The number of discrete wavefronts were calculated for each field of view and tracked over its lifespan. Wavefronts smaller than 20 pixels (approximately 14mm) and lasting less than 2ms were treated as noise and not included in the analysis. Wavefront collision was defined as a phenomenon wherein two or more wavefronts collided with each other and merged into a single wavefront (Video I). Wavefront fractionation was defined as a phenomenon where a single wavefront would split into two or more wavefronts (Video II). A collision or a fractionation marked the end of the lifespan of a wavefront. Alternately, wavefront tracking was also terminated if the wavefront moved past the field of view, fell below the 20-pixel threshold or expired (Video III). Wavefronts that were at least 50 pixels in length (approximately 35 mm) were also tracked for multiplicity and repeatability. Multiplicity was defined as an index of number of unique wavefront pathways in an overall activation pattern. A wavefront pathway was classified as unique, if it lasted at least

10 ms. Repeatability was defined as measure of the number of times a wavefront propagation over a pathway was repeated (Video IV). Well-organized rhythms such as monomorphic ventricular tachycardia (MVT) would be expected to have high repeatability compared to complex rhythms such as ventricular fibrillation (VF).

Phase singularities (PS) were calculated as nonzero topological charges constrained to the isophase wavefronts within 3-pixel radius (approximately 2mm) in each frame. PS were considered distinct if they were >3 pixels apart in a single frame. Moreover, PS with lifespan of < 20 ms were treated as false positives and not included in the analysis. Stable PS were arbitrarily defined as lasting at least 1 cycle length. PS meandering (total distance traveled) and PS displacement (shortest path between initial and final position) were calculated by tracking individual PS trajectories across their lifespans.

To evaluate endo/epi dissociation dynamics, wavefronts, PS, DF, RI, and OI were compared between the two surfaces. The spatio-temporal autocorrelation evaluation of epicardial and endocardial wavefronts entailed time aligning the two wavefronts and then comparing them for similarity using a combination of Fréchet distance and pair-wise Euclidean distance over each time frame of their individual lifespans. Fréchet distance is a measure of similarity between two curves that takes into account the continuity of shapes, whereas pair-wise Euclidean distance measures the proximity between the two curves. The wavefronts were considered similar if the median Fréchet distance was < 20 pixels (approximately 14 mm) and the median Euclidean distance was < 10 pixels (approximately 7 mm). The thresholds were arbitrarily chosen after visual inspection of the wavefronts. Similarly, the epicardial and

endocardial PS were time aligned and their trajectories compared using pair-wise Euclidean distance over each time frame of their lifespans. The PS were considered similar if the median pair wise Euclidean distance was less than 10 pixels (approximately 7 mm). Epicardial and endocardial DF, RI, and OI were compared at each pixel location to compute the Jaccard similarity index, which measures the similarity between two sets of data. The Jaccard index is formally defined as the size of the intersection divided by the size of the union of the two data sets.

Electrical Cardiac Mapping

To establish clinical relevance of optical mapping we applied simultaneous electrical and optical cardiac mapping in donor hearts (n=3; male=2, female=1). Briefly, two stretchable passive electrode arrays were used for epicardial and endocardial electrical mapping. Each array (3cm x 4cm) had 64 electrodes arranged in an 8x8 matrix with interelectrode distance of approximately 3-4mm and electrode diameter of approximately ~1mm.

Fabrication of 64 electrode stretchable passive array was done in John Rogers lab at Northwestern University based on a previous design. Briefly, the process entailed starting with coating and curing a thin layer of PDMS (10 µm, Dow Corning) on a glass substrate followed by oxygen plasma treatment. Another coating and curing process formed a layer of polyimide (2 µm; HD Microsystem) on top of PDMS. Depositing chromium (5 nm) and gold (300 nm) films using electron-beam evaporation followed by lithographic patterning and etching yielded mesh electrodes and conductive traces. An overcoat of a layer of polyimide (2 µm) placed the metal wires into the mechanical neutral plane, and subsequent lithographic patterning and oxygen

plasma treatment defined matching patterns with exposed electrode surfaces. A cellulose-based water-soluble tape (3M) retrieved the resulting structures from the glass substrate. Attaching the tape to a layer of Ecoflex (8 μm; Smooth-On) with an adhesive silicone surface (80 μm; RT GEL 4642, Bluestar) on a PET substrate and dissolving the tape completed the transfer of the electrode arrays. The resulting electrode array was an 8 x 8 matrix with dimensions of 3cm x 4cm. Each electrode was sized at 1mm in diameter and the interelectrode distance between 3mm and 4mm.

For electrogram mapping, a customized printed circuit board (PCB) board was fabricated in John Viventi's lab at Duke University based on a previous design. Briefly, the head stage was constructed from off-the-shelf integrated circuits and specifications suitable for inexpensive PCB manufacturing and assembly. Electrode contacts were routed from the ZIF connector to 30 dual op-amps in a unity gain configuration (OPA2376, Texas Instruments). The 60 outputs of these buffers were multiplexed by a pair of dual 16:1 multiplexer (ADG726, Analog Devices, Inc.). The outputs of the multiplexers were high-pass filtered at 0.0016 Hz to remove the average electrode DC offset and subsequently amplified by a pair of dual op-amps with 20× gain (OPA2376, Texas Instruments). All signal and interface wires were carried by an ultra-flexible μHDMI cable (Draco Electronics, LLC, CA, US) with analog signals measured differentially on the shielded, twisted pairs. The PCB board connected to the Intan 1024ch recording controller through two 36-pin wire adapters, a 64-channel amplifier board (RHD2164), and a serial peripheral interface cable. A commercial software interface simultaneously recorded electrograms from 64 channels at a sampling rate of 20 kS s^{-1}. The bandwidth of the amplifier

hardware extended from 0.1 to 200 Hz. A notch filter at 60 Hz further reduced the noise signal from electrical wires.

Synchronized measurements of electrograms from the Intan recording controller and optical signals from the MiCAM05 exploited the MARK OUT port from the Intan system. The MARK OUT port sent a digital pulse to trigger the optical mapping. One Power Lab computer interface recorded the ECG through commercial electrodes, provided electrical output to another commercial electrodes for pacing and generated a trigger signal using the TRIGGER port at the start of the measurement. The schematic of electrode array connection to the IntanTech DAQ system is shown in the attached pdf file.

All the unipolar electrical signals were processed in MATLAB version 2020a. The local activation times were determined by calculating the time of dV/dt_{min}. which corresponds to the steepest downward slope in the activation complex. The local repolarization times were determined by calculating T_{up}, the point in the T wave with the maximum upward slope (Supplementary Figure IIC). Activation-recovery interval (ARI) was computed as the interval between local activation and repolarization time. Activation-recovery interval (ARI), a surrogate marker of APD, was then computed as the interval between local activation and repolarization time and is assumed to occur near APD50.

Transcriptome

Tissues from RVOT and RV apical region, separated into epicardium and endocardium (total hearts=10, male=5, female=5; each heart=4 tissue samples) were collected from donor hearts

and preserved in RNAlater (Invitrogen) for 24h at 4°C and then transferred to -80°C until subsequent RNA extraction. RNA was extracted with RNeasy Fibrous Tissue Mini Kit (Qiagen) according to manufacturer's protocol using 40 mg of tissue. RNA sequencing was performed with Illumina HiSeq using paired-end 150 reads (Novogene). Reads were aligned with Minimap2 (10.1093/bioinformatics/bty191) in Galaxy Project (https://usegalaxy.org/) using built-in reference genome hg38 and paired end reads setting. Read were counted with featureCounts (10.1093/bioinformatics/btt656). DESeq2 was used for differential gene expression (10.1186/s13059-014-0550-8). Differentially expressed genes (DEGs) cutoff was at *padj<0.05*. Enrichment analysis on DEGs was performed with goana (10.12688/f1000research.8987.2) for gene ontology and clusterProfiler (10.1089/omi.2011.0118) for KEGG.

Immunostaining

Fixed specimens of the human heart RVOT were shipped to ETSU at 4 ºC in PBS containing 20% sucrose and 0.02% sodium azide. Samples were dissected, frozen on dry ice, and stored at -80 ºC. 30 μm thick sections were cut at -20 to -25°C using a Leica CM3050S cryostat (Leica Microsystems Inc., Bannockburn, IL, USA) and collected on charged slides. Tissues were sectioned in a transmural plane from epicardium to endocardium, and sections were collected to yield four representative sets of slides spanning the same volume of tissue. After drying at room temperature (RT), the slides were then stored at -20 °C.

Slide-mounted tissue sections were immunostained at RT for specific neural markers using standard methods of ABC immunohistochemistry. Slides were rinsed with PBS (pH 7.3), incubated for 10 min in PBS containing 0.4% Triton X-100 and 0.5% bovine serum albumin (BSA), treated for

15 min with 1.0% H_2O_2 in PBS, rinsed an additional time with PBS and incubated 10 min in PBS containing 0.4% Triton X-100 and 0.5% BSA. Slides were then placed in an incubation box and covered with blocking buffer (PBS containing 1% BSA, 0.4% Triton X-100, and normal serum (VECTASTAIN® ABC-HRP Kit, Peroxidase (Goat IgG) PK-4005 or VECTASTAIN® ABC-HRP Kit, Peroxidase (Rabbit IgG) PK-4001). After 2 hours, the blocking buffer was replaced with fresh blocking buffer containing one of three primary antibodies: rabbit anti-vesicular acetylcholine transporter (VAChT, Synaptic Systems, Cat. No. 139103, 1:500), sheep anti-tyrosine hydroxylase (TH, Millipore Cat. No. AB1542, 1:500), or rabbit anti-protein gene product 9.5 (PGP9.5, Abcam Cat. No. ab108986, 1:2000) and incubated overnight at RT. Sections were washed with PBS and PBS containing 0.5% BSA followed by a two-hour incubation in biotinylated secondary antibodies (1:200 dilution) from the kits. Slides were washed again, before a 1.5-hour incubation with the ABC reagent from the kits. Slide were next washed for 20 min in 50 mM Tris buffer (pH7.6) before treatment for 1-10 min with the chromogen (Vector ImmPACT VIP Kit, SK4605) to visualize localization of the markers. Slides were washed, dehydrated and cover glasses attached using Cytoseal XYL (Thermo Scientific Cat. No. 8312-4).

For each RVOT, slides labeled for TH, VAChT, or PGP9.5 were viewed, and digital images collected with an Olympus BX41 microscope equipped with an Olympus DP74 digital camera and cellSens software (Olympus America Inc., Center Valley, PA). For each stain, two representative images of sub-epicardium and sub-endocardium were collected per section. This was repeated for a total of 4 sections, yielding a total of 16 images per sample for each stain. Each image was taken as an EFI (Extended Focus Image) using a 20x objective.

Using ImageJ Software (NIH, USA), the nerve fiber density threshold was measured. Nerve density was calculated as the area occupied by nerves as a percentage of the entire image area and reported as % area. The average of three such measurements was determined and combined with readings from other sections to get a single value for nerve density for that marker in the sub-epicardium and sub-epicardium of that sample. Combined data were analyzed and graphed using Prism version 8.4.3 (GraphPad Software, San Diego, CA).

Statistical analysis

All means characterizing the spatial average of a single study are represented as sample mean$\pm$SD. All means that characterize average trends across the cohort of donor hearts are reported as sample mean$\pm$SEM. Repeated measures ANOVA (one-way or two-way) with multiple comparisons and post hoc Holm-Sidak or Tukey's Honest Significant Difference (THSD) multiple comparison test was used for APD and PVC comparisons respectively. Two-tailed paired t test was used for comparison between epicardial and endocardial WF and PS metrics. Significance was defined as $p<0.05$.

Figure Legends

Supplementary Figure I. Donor human heart information

Table of donor human heart information including age, sex, race, cause of death (COD), left ventricular ejection fraction (LVEF), body mass index (BMI), and relevant clinical history including drug, alcohol, nicotine (cigarette smoker) use, diabetes (DM), hypertension (HTM), and heart disease such as sinus tachycardia, left ventricular hypertrophy (LVH), coronary arterial disease (CAD), and myocardial infarction (MI).

Supplementary Figure II. Optical action potential and electrogram feature extraction

A: Calculation of APD80% from local action potential. **B:** Calculation of activation recovery interval from local electrogram. **C:** Transformation of local action potentials into phase domain for arrhythmia analysis.

Supplementary Figure III. Comparison of optical and electrical restitution curves

A: Epicardial electrical and optical restitution curve. **B:** Endocardial electrical and optical restitution curve. **C:** APD50 and ARI correlation at 30BPM. **D:** APD50 and ARI correlation at 60BPM. **E:** APD50 and ARI correlation at 120BPM. **F:** APD50 and ARI correlation at 240BPM.

Supplementary Figure IV. Restitution curves for Group 1 and Group 2 donor hearts

A: Group 1 epicardial and endocardial RVOT and RV apical region restitution curves under baseline conditions and after treatment with isoproterenol (100 nM) or acetylcholine (100 μM).

B: Group 2 epicardial and endocardial RVOT and RV apical region restitution curves under baseline conditions and after treatment with isoproterenol (100 nM) and acetylcholine (100 μM).

Supplementary Figure V. Immunostained RVOT section

Nerve density distribution in RVOT tissue section from a representative donor heart (D27) using immunohistochemical staining.

Supplementary Figure VI. Concordant Alternans

A: Representative example of concordant alternans in donor human heart (D11) when paced at 300BPM. Corresponding local action potentials and endocardial alternans (APD50) map are shown. **B:** Plots of APD50 alternans locations and that of the frequency of concordant and discordant alternans observed are shown.

Supplementary Figure VII. Epicardial and endocardial wavefront temporal series

A: Temporal series of epicardial and endocardial wavefronts from donor heart (D14) paced at 120BPM. **B:** Temporal series of epicardial and endocardial wavefronts from donor heart (D4) paced at 120BPM.

Supplementary Figure VIII. Summary of arrhythmia statistics by sex

A: Dominant frequency **B:** Regularity index **C:** Organization index **D:** Number of wavefronts per unit area per unit time. **E:** Average size of the wavefronts **F:** Average duration of the wavefronts. **G:** Percentage of wavefronts that terminated with collisions. **H:** Percentage of wavefronts that terminated with fractionations (wavefront splitting into two or more wavefronts). **I:** Percentage of wavefronts that were unique (multiplicity). **J:** Percentage of wavefronts that repeated their trajectories (repeatability). **K:** Number of PS per unit area per unit time. **L:** Average duration of PS. **M:** Average path length of the PS trajectory. **N:** Average distance traveled by the PS. **O:** Dynamic time warp. **P:** Jaccard similarity index.

Supplementary Figure IX. Transcriptome profile of human RVAR

A: Hierarchical clustering of both genes and the samples based on the gene expression profile (DEGs) in the gene expression matrix, identifying the top 20 genes. **D:** GO analysis.

Video Legends

Video I. Wavefront collision

Representative example of wavefront collision. Wavefront of interest is marked in orange.

Video II. Wavefront fractionation

Representative example of wavefront fractionation. Wavefronts of interest are marked in orange.

Video III. Wavefront expiration

Representative example of wavefront expiration. Wavefront of interest is marked in orange.

Video IV. Wavefront repeatability

Representative example of wavefront repeatability. Wavefronts of interest are marked in orange.

Video V. Monomorphic ventricular tachycardia

Representative example of MVT seen in donor human heart (D14).

Video VI. Ventricular fibrillation

Representative example of VF seen in donor human heart (D4)

Supplementary Figure I

Mode	Group	Donor #	Age	Sex	Race	COD	LVEF	BMI	Drugs	Alcohol	Smoker	DM	HTN	Heart Disease
	Group 0	D1	62	M	Black	Brain Death	NA	23.3	Yes	Yes	Yes	No	No	No
		D2	65	F	White	Stroke	NA	36.3	No	Yes	Yes	No	Yes	No
		D3	71	F	White	Stroke	65%	26.6	No	Yes	No	No	No	No
Functional Data	Group I	D4	63	F	White	Stroke	NA	26.9	No	No	No	No	No	Sinus Tac
		D5	49	M	Hispanic	Head T	70%	36.3	No	Yes	Yes	No	No	Mild LVH
		D6	35	F	Asian	Stroke	65%	31.7	No	Yes	No	No	No	No
		D7	57	M	Black	Stroke	NA	40.2	No	Yes	No	No	Yes	No
		D8	57	F	Black	Stroke	70%	29.2	No	Yes	Yes	No	No	No
		D9	62	M	Hispanic	Stroke	NA	18.6	No	Yes	Yes	Yes	No	No
		D10	68	F	Black	Brain Death	60%	30.4	No	No	No	No	Yes	Mild LVH
	Group 2	D11	59	F	Black	Stroke	65%	38.3	No	Yes	Yes	Yes	Yes	CAD
		D12	60	F	White	Brain Death	NA	30.8	No	No	Yes	No	No	Sinus Tac
		D13	56	M	White	Brain Death	55%	26.9	Yes	Yes	Yes	Yes	No	Sinus Tac
		D14	51	M	White	Stroke	NA	21.5	Yes	Yes	Yes	No	No	MI
		D15	62	M	White	Stroke	NA	23	Yes	Yes	Yes	No	No	No
		D16	61	F	White	Stroke	70%	23.9	Yes	Yes	Yes	No	Yes	Mild LVH

Mode	Group	Donor #	Age	Sex	Race	COD	LVEF	BMI	Drugs	Alcohol	Smoker	DM	HTN	Heart Disease
Molecular Data	RNASeq	D17	54	M	Hispanic	Brain Death	60%	28.3	No	Yes	No	No	No	AF
		D18	47	M	Asian	Brain Death	30%	23.9	No	Yes	Yes	No	No	No
		D19	39	M	Hispanic	Stroke	NA	32.1	Yes	Yes	Yes	No	No	ST Abnorm
		D20	52	M	White	Brain Death	NA	29.1	Yes	Yes	Yes	No	Yes	No
		D21	51	M	White	Head Trauma	65%	39.2	Yes	Yes	Yes	No	Yes	ST Abnorm
		D22	36	F	Asian	Stroke	NA	31.7	No	Yes	No	Yes	No	No
		D23	49	F	Asian	Head Trauma	65%	19.4	No	No	No	No	No	No
		D24	53	F	Black	Stroke	70%	30.1	NA	NA	NA	NA	NA	No
		D25	45	F	White	Stroke	NA	38.3	NA	NA	NA	NA	NA	No
		D26	49	F	Hispanic	Stroke	NA	35	No	No	No	No	No	No
Structural Data	Immuno-Staining	D27	52	M	White	Head Trauma	NA	35.7	No	Yes	Yes	No	No	No
		D28	49	F	Hispanic	Stroke	65%	48.2	NA	NA	NA	NA	NA	NA
		D29	48	F	Black	Stroke	NA	41.4	No	No	Yes	No	Yes	CAD
		D30	71	F	Asian	Stroke	NA	36.3	No	No	No	No	Yes	No

Supplementary Figure II

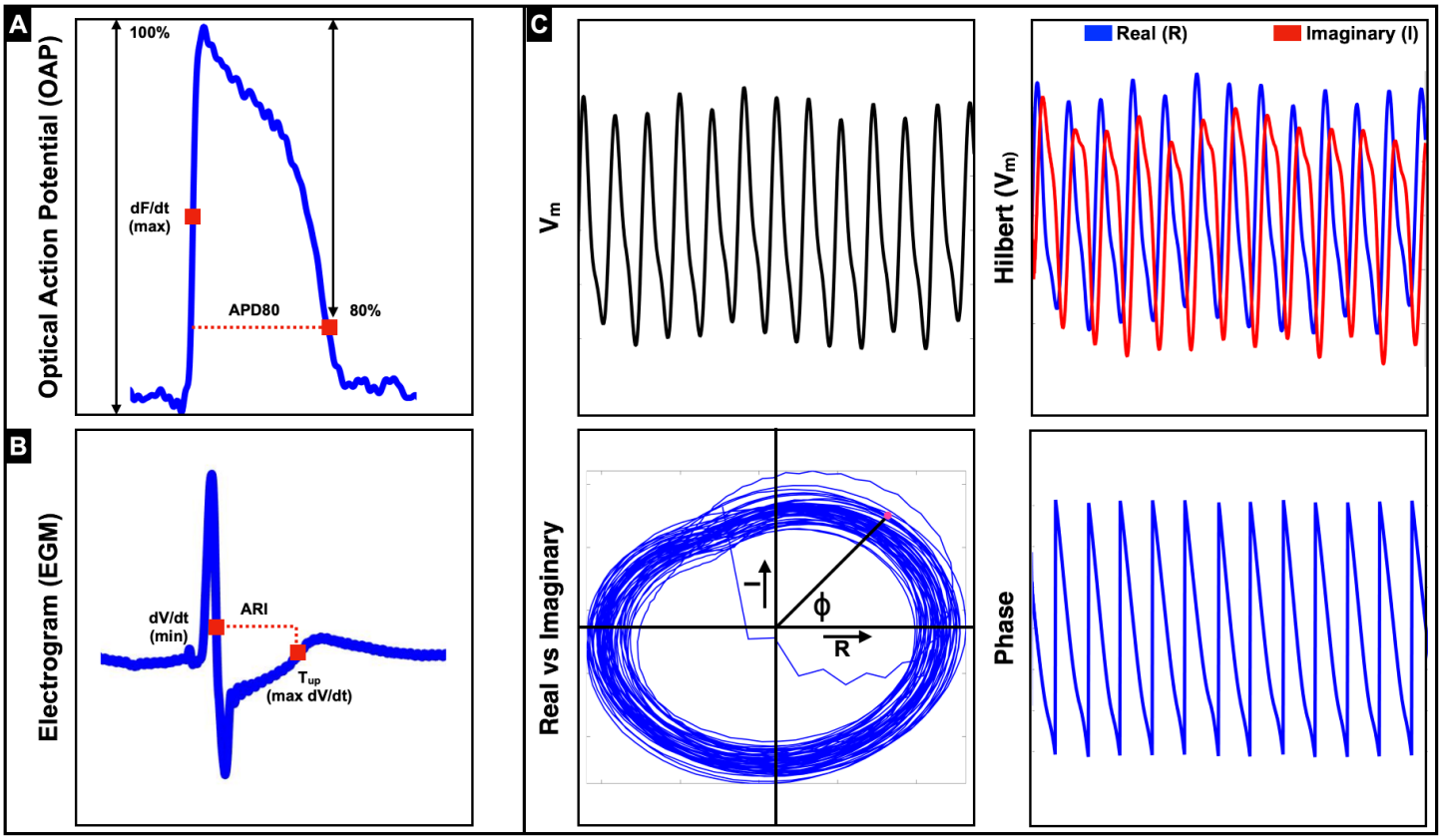

Supplementary Figure III

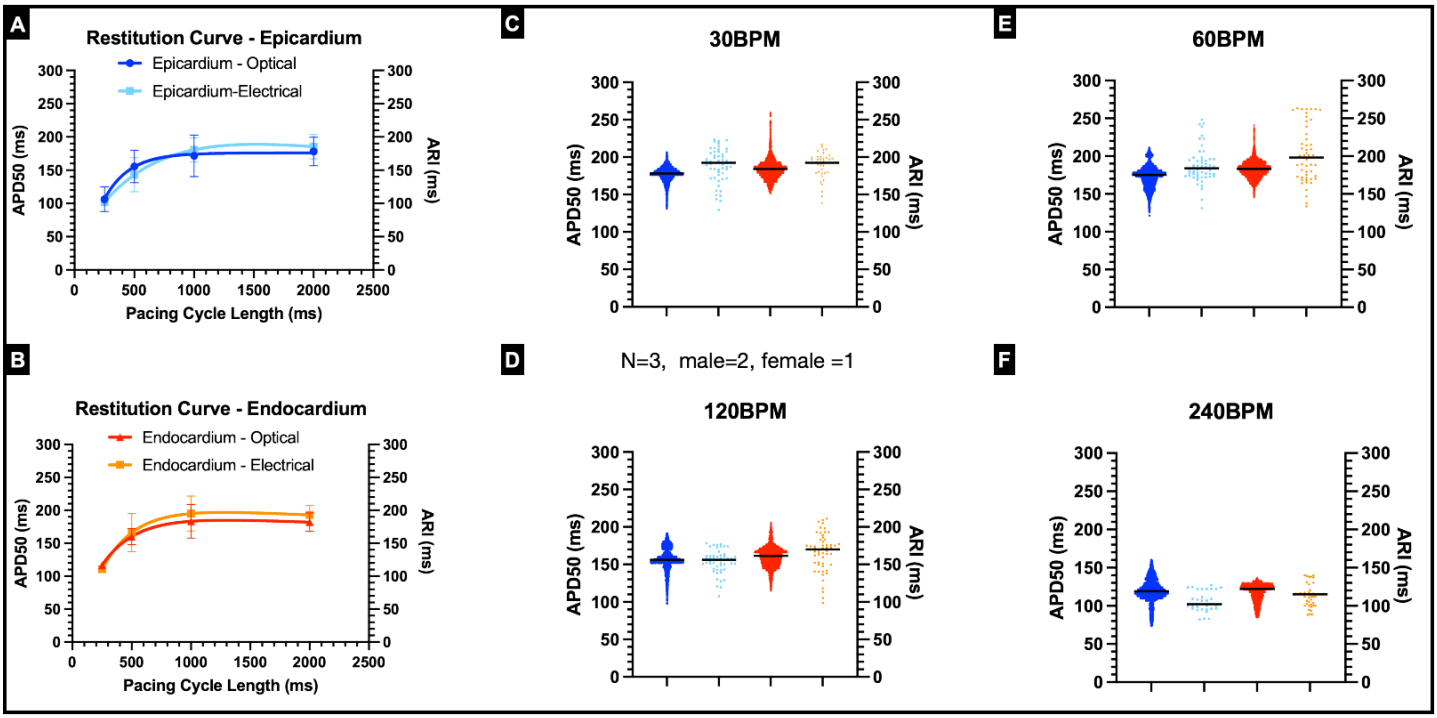

Supplementary Figure IV

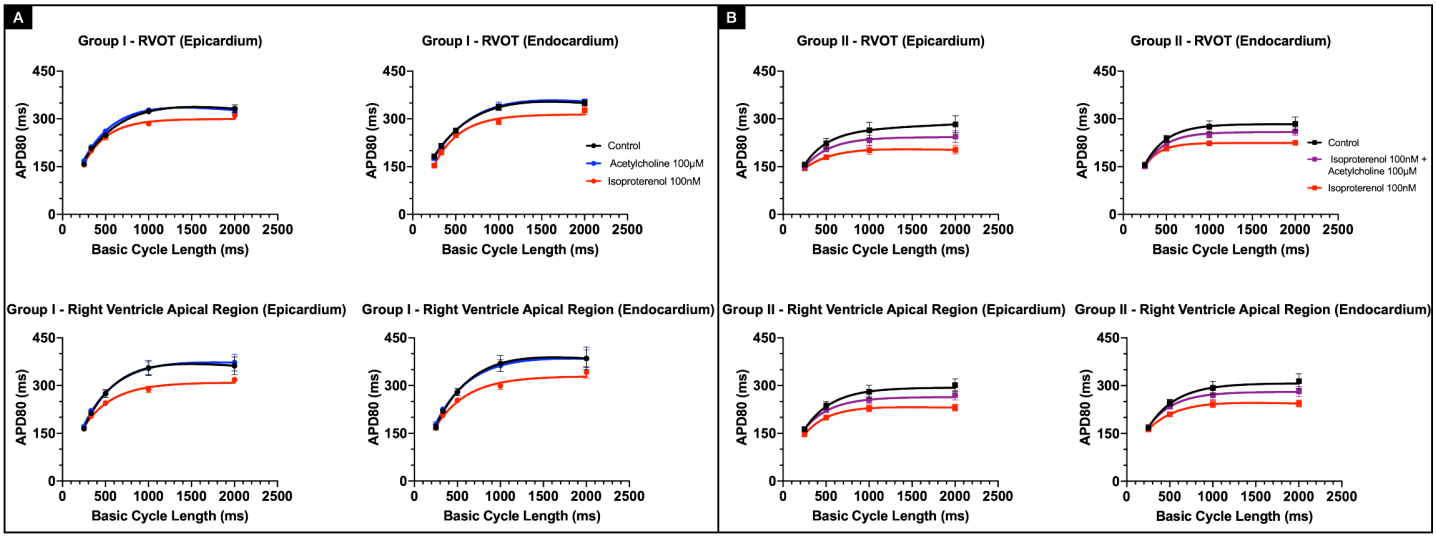

Supplementary Figure V

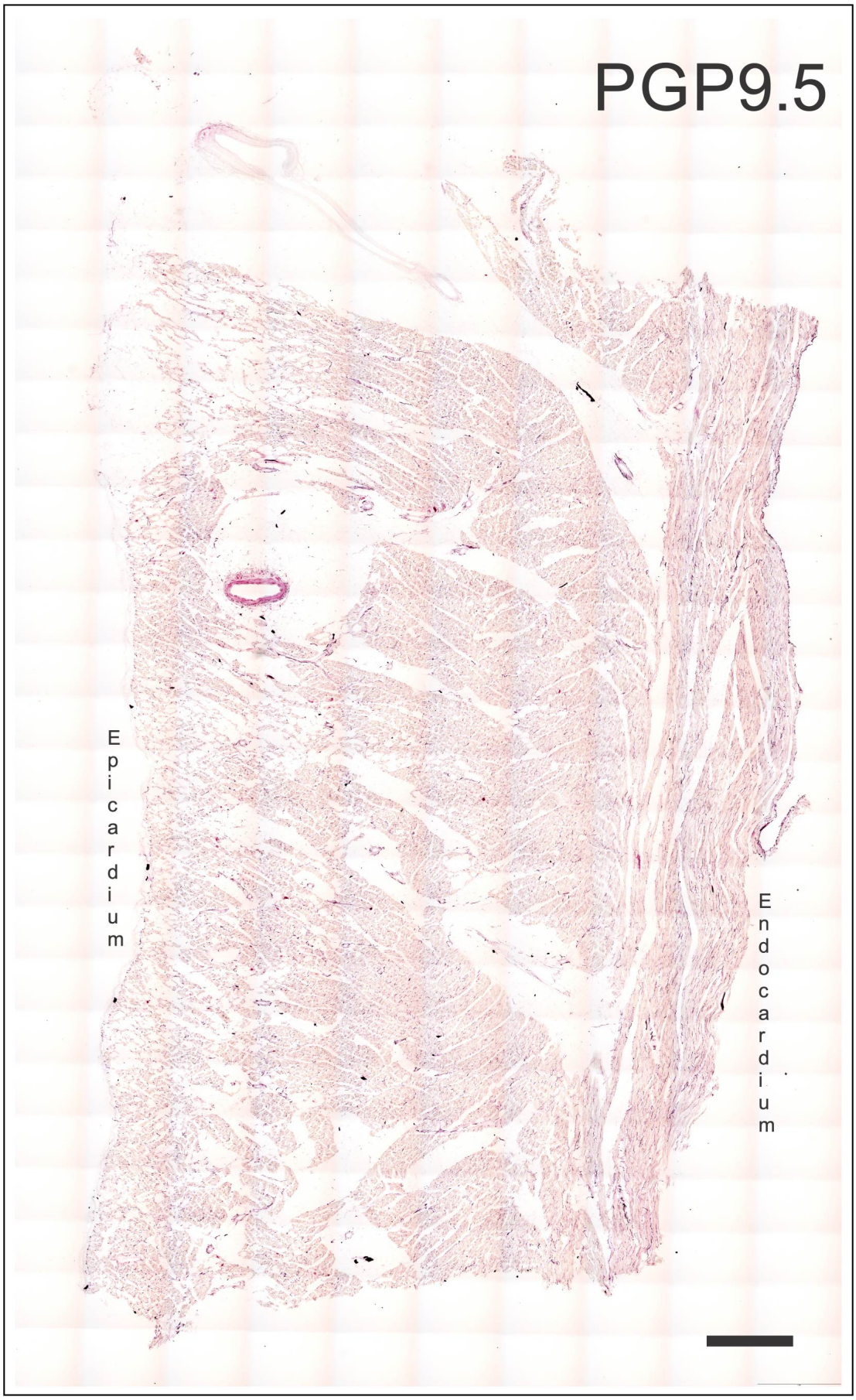

Supplementary Figure VI

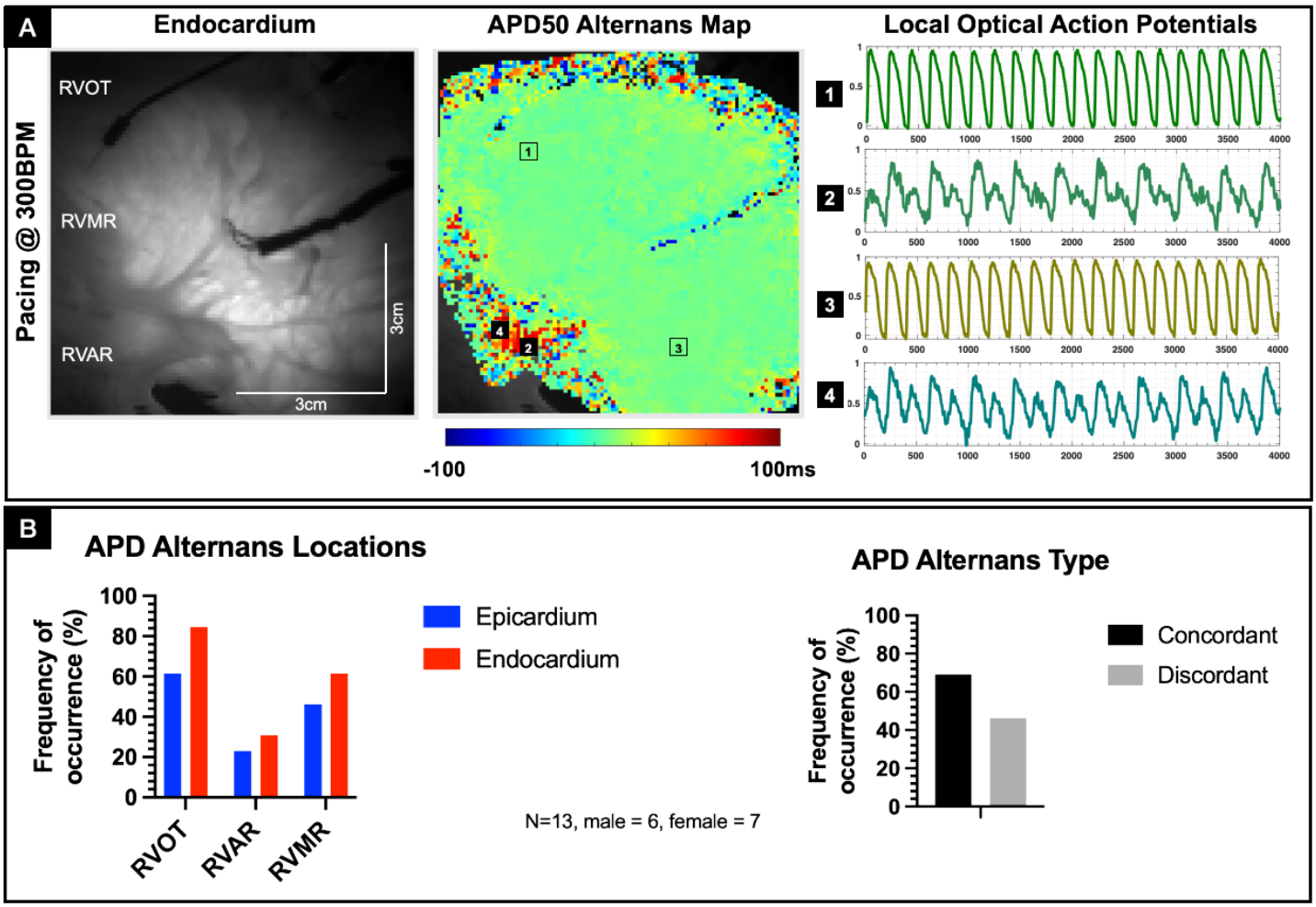

Supplementary Figure VII

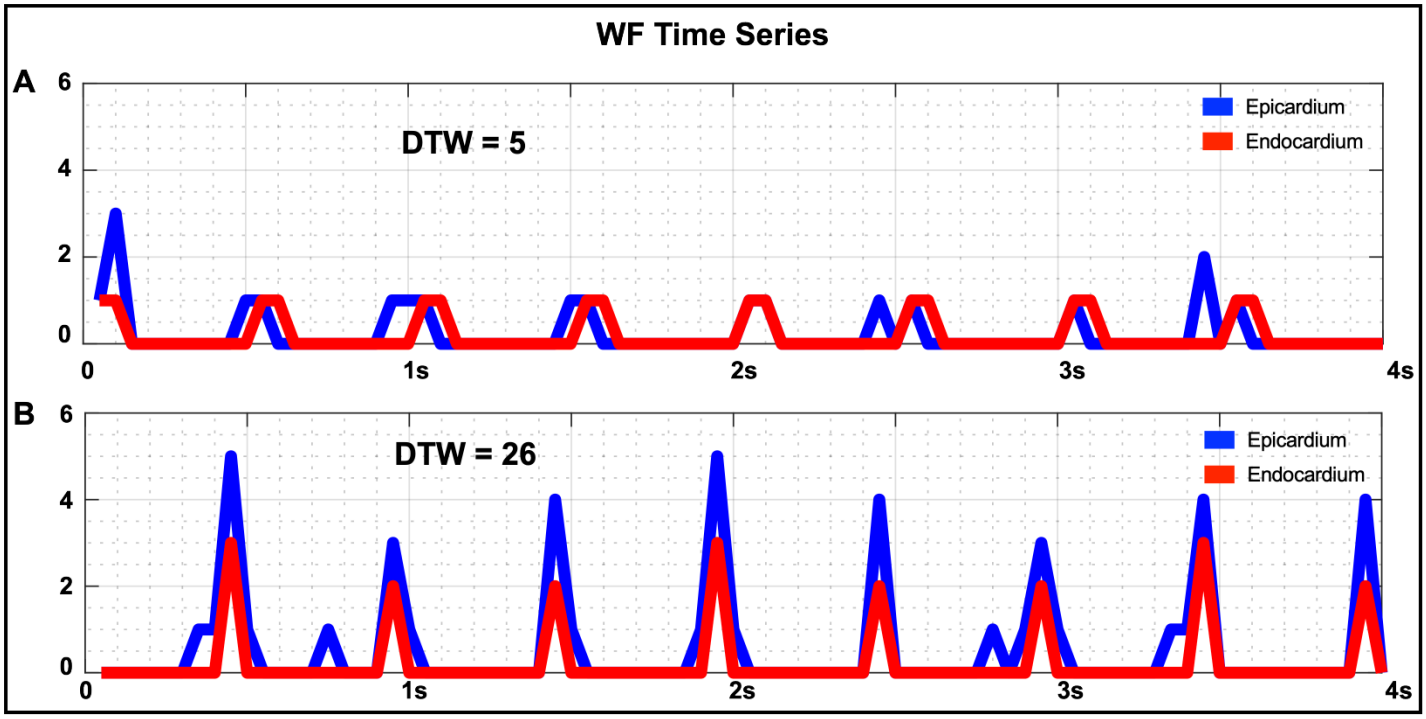

Supplementary Figure VIII

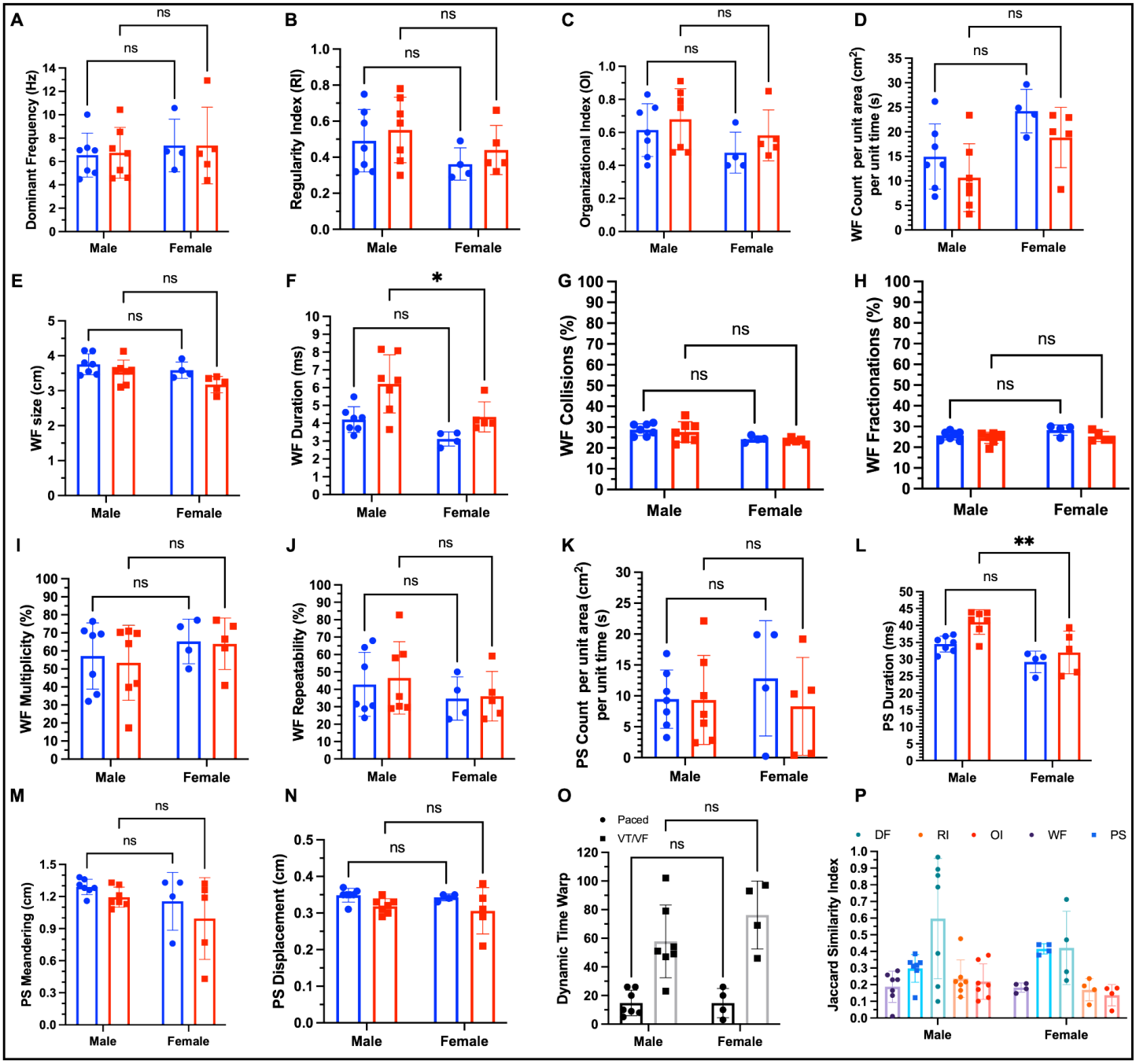

Supplementary Figure IX

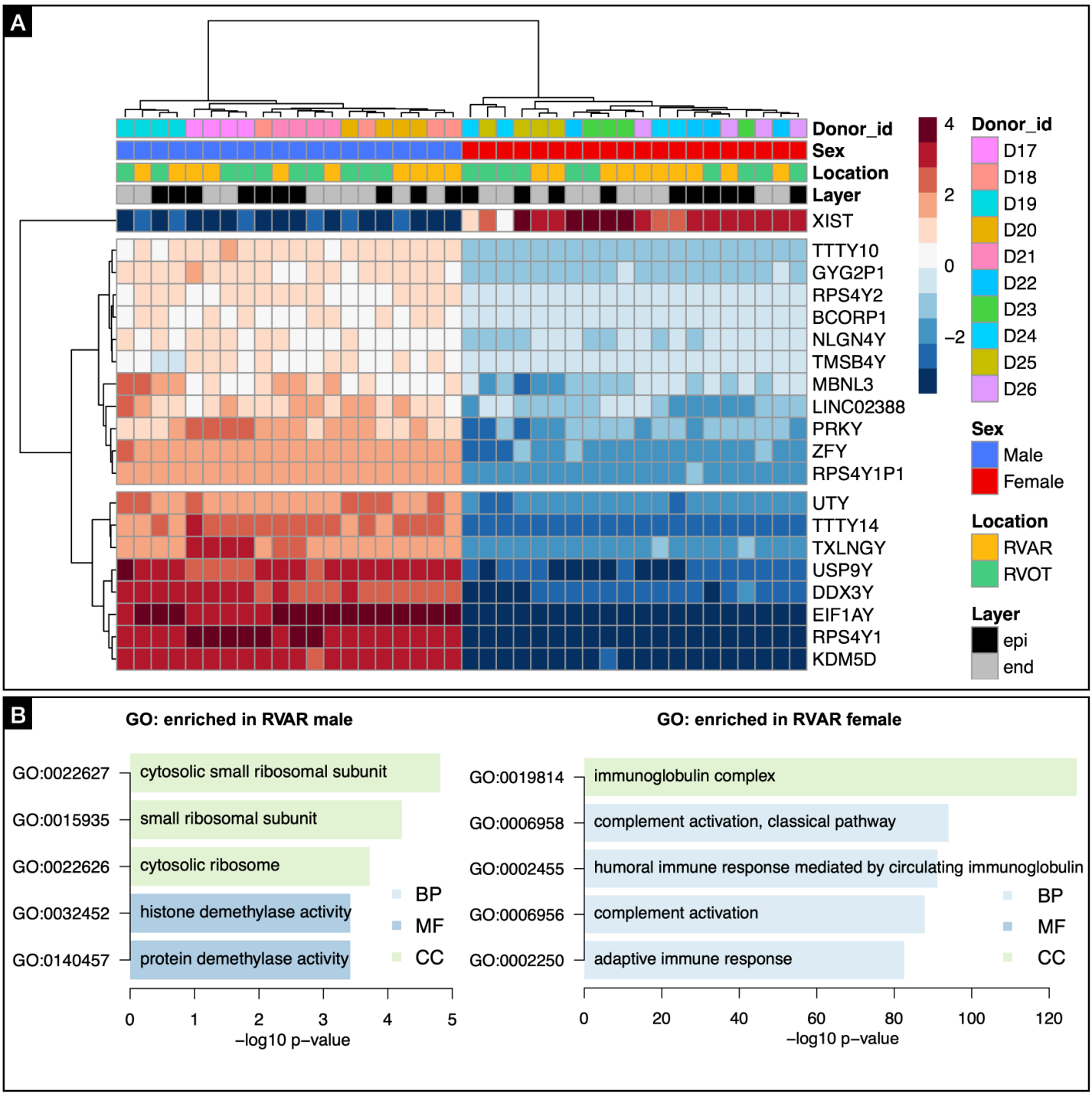

Mapping

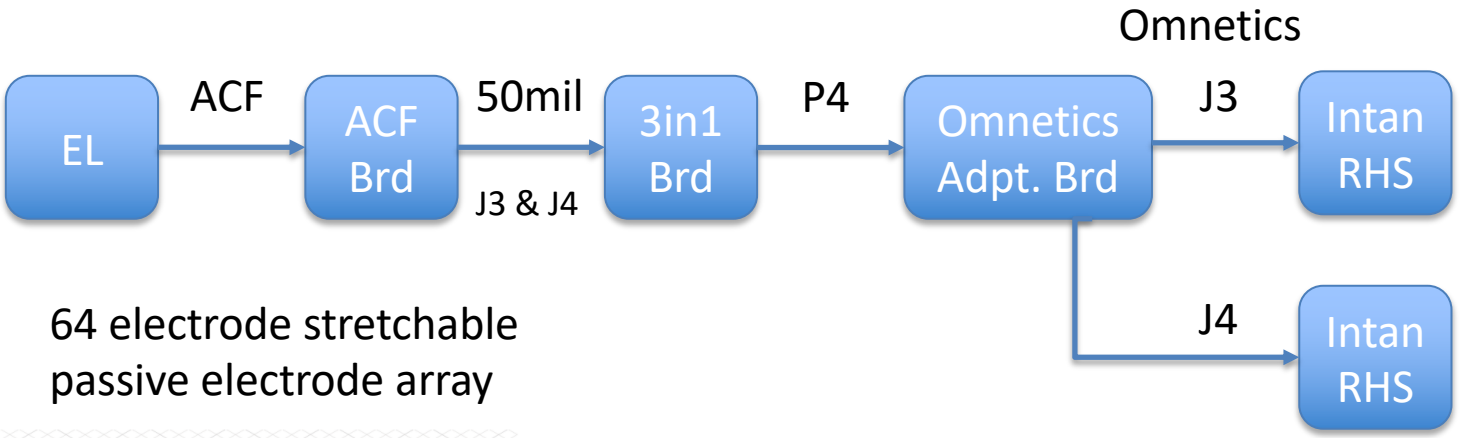

64 electrode stretchable passive electrode array

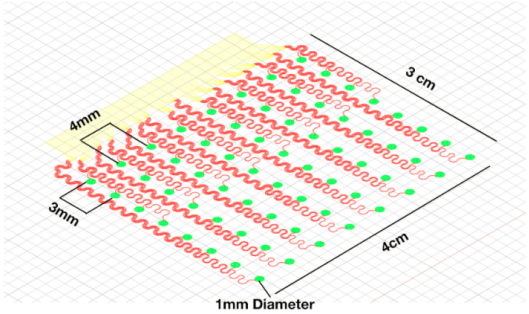

***NOTE:**

Electrode mapped as "face-up"

(i.e. if you are looking at the exposed electrode metal contacts, A1 is on the top left.)

		ACF64 Brd	P4 to Omne. Adpt.		
	Electrode		3 in 1 Test Brd		Intan RHS 2132
	EL	ACF	50 mil	P4	Omnetic	Intan
	B2	51	J4-14	45	J3-10	
	B7	55	J4-6	61	J3-11	
	A6	62	J4-13	43	J3-12	
	A4	57	J4-3	63	J3-13	
	B3	50	J4-16	41	J3-14	
	D8	40	J3-4	65	J3-15	
	A7	63	J4-15	39	J3-16	
GND	G4	9	J4-34	3	J3-17	
	B4	49	J4-18	37	J3-18	
	F8	24	J3-33	5	J3-19	
	A8	64	J4-17	35	J3-20	
	H7	7	J4-31	7	J3-21	
	G8	16	J4-20	33	J3-22	
	G3	10	J4-32	9	J3-23	
	H4	1	J4-19	31	J3-24	
	H6	6	J4-29	11	J3-25	
	G7	15	J4-22	29	J3-26	
	G2	11	J4-30	13	J3-27	
	H3	2	J4-21	27	J3-28	
	H5	5	J4-27	15	J3-29	
	B5	53	J4-10	53	J3-3	
	G6	14	J4-24	25	J3-30	
	G1	12	J4-28	17	J3-31	
	H2	3	J4-23	23	J3-32	
	H1	4	J4-25	19	J3-33	
	G5	13	J4-26	21	J3-34	
	A1	60	J4-9	51	J3-4	
	A2	59	J4-7	55	J3-5	
	B1	52	J4-12	49	J3-6	
	B6	54	J4-8	57	J3-7	
	A5	61	J4-11	47	J3-8	
	A3	58	J4-5	59	J3-9	
	E6	30	J3-24	26	J4-10	
	E2	27	J3-30	14	J4-11	
	F3	18	J3-21	28	J4-12	
	F5	21	J3-27	16	J4-13	
	E7	31	J3-22	30	J4-14	
	E1	28	J3-28	18	J4-15	
	F4	17	J3-19	32	J4-16	
GND	B8	56	J4-4	36	J4-17	
	E8	32	J3-20	34	J4-18	
GND	H8	8	J4-33	68	J4-19	
	C8	48	J3-17	38	J4-20	
	C1	44	J3-9	54	J4-21	
	D4	33	J3-18	40	J4-22	
	D5	37	J3-10	56	J4-23	
	C7	47	J3-15	42	J4-24	
	C2	43	J3-7	58	J4-25	
	D3	34	J3-16	44	J4-26	
	D6	38	J3-8	60	J4-27	
	C6	46	J3-13	46	J4-28	
	C3	42	J3-5	62	J4-29	
	E4	25	J3-34	6	J4-3	
	D2	35	J3-14	48	J4-30	
	D7	39	J3-6	64	J4-31	
	C5	45	J3-11	50	J4-32	
	C4	41	J3-3	66	J4-33	
	D1	36	J3-12	52	J4-34	
	F1	20	J3-25	20	J4-4	
	F7	23	J3-31	8	J4-5	
	E5	29	J3-26	22	J4-6	
	E3	26	J3-32	10	J4-7	
	F2	19	J3-23	24	J4-8	
	F6	22	J3-29	12	J4-9	

ACF Connection

ACF pin1

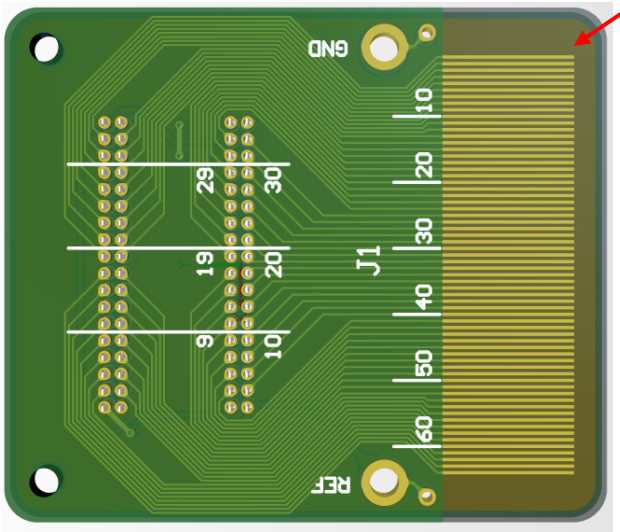

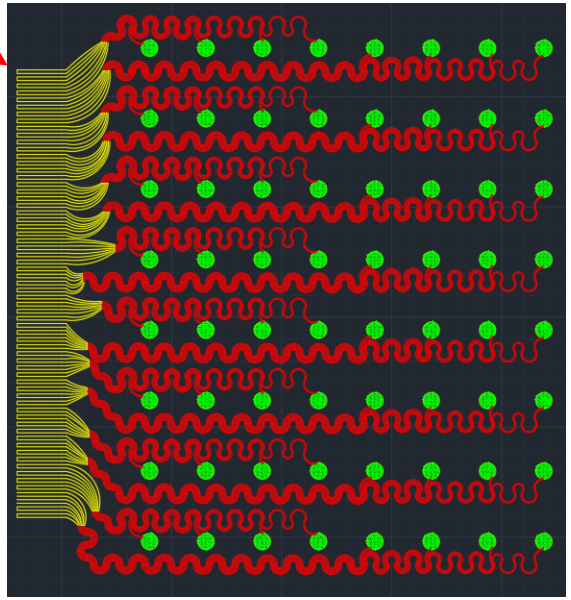

50mil Connection

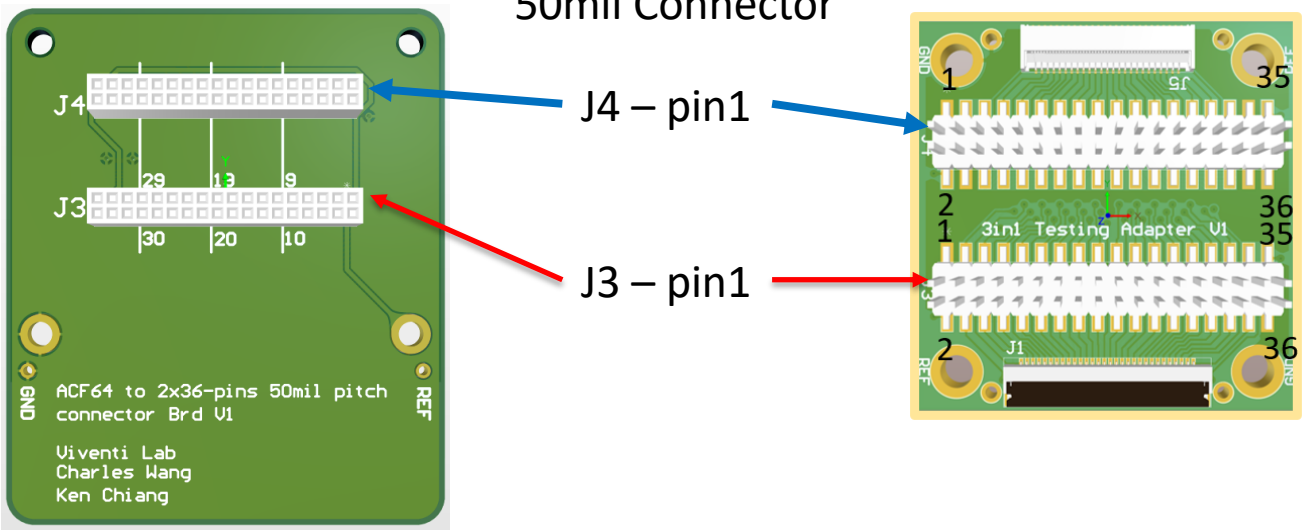

***NOTE:**
Pin1 should be connected to each other.
J3 → J3
J4 → J4

P4 Connection

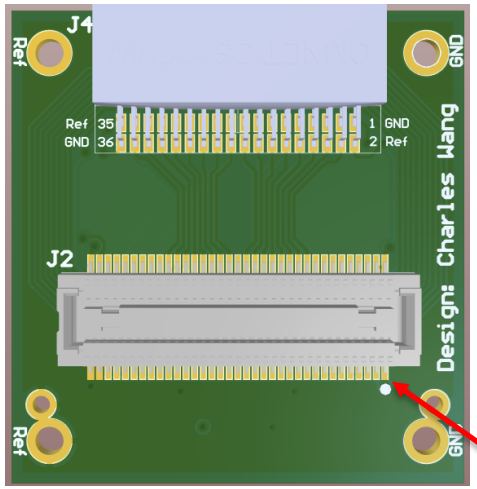

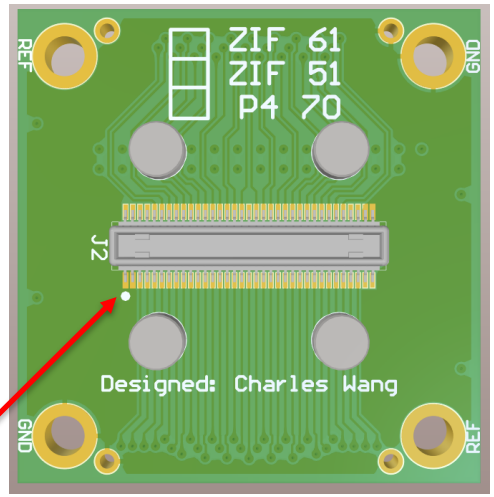

P4
pin1

***NOTE:**
Pin1 should be connected to each other
(i.e. after connection, the two white dots should aligned and on top of each other)

Omnetics Connection

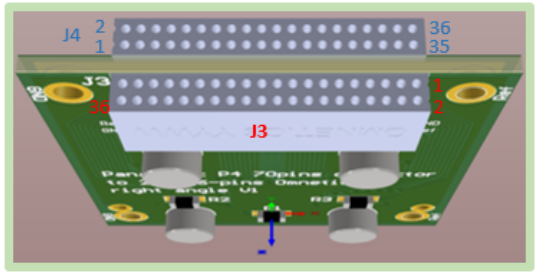

Omnetics pin number

J4	2	4	6	8	10	12	14	16	18	20	22	24	26	28	30	32	34	36
	1	3	5	7	9	11	13	15	17	19	21	23	25	27	29	31	33	35
J3	35	33	31	29	27	25	23	21	19	17	15	13	11	9	7	5	3	1
	36	34	32	30	28	26	24	22	20	18	16	14	12	10	8	6	4	2

Corresponding electrode contact on each omnetices pin

J4	REF	F1	E5	F2	E6	F3	E7	F4	E8	C8	D4	C7	D3	C6	D2	C5	D1	GND
	GND	E4	F7	E3	F6	E2	F5	E1	B8	H8	C1	D5	C2	D6	C3	D7	C4	REF
J3	REF	H1	G1	H5	G2	H6	G3	H7	F8	G4	D8	A4	B7	A3	B6	A2	B5	GND
	GND	G5	H2	G6	H3	G7	H4	G8	A8	B4	A7	B3	A6	B2	A5	B1	A1	REF

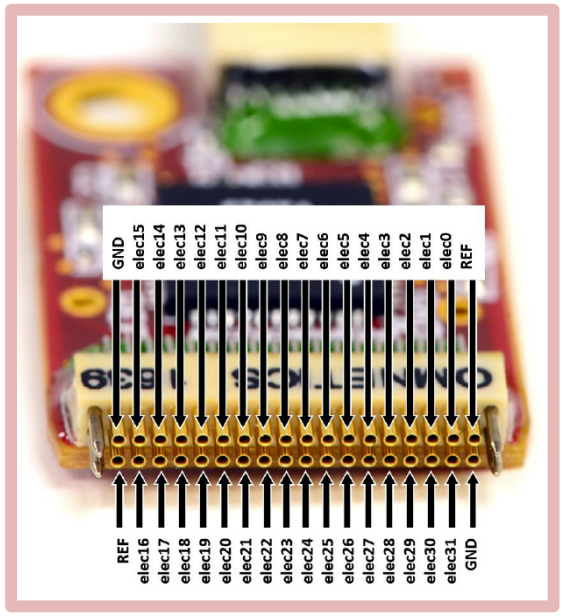

*Final Intan channel mapping depends on how the orientation of the 2x Intan headstages connected.

	ACF64 Brd	P4 to Omne. Adpt.		
	Electrode	3 in 1 Test Brd	Intan RHS 2132	
	EL	ACF	50 mil	P4	Omnetic	Intan
	B2	51	J4-14	45	J3-10	
	B7	55	J4-6	61	J3-11	
	A6	62	J4-13	43	J3-12	
	A4	57	J4-3	63	J3-13	
	B3	50	J4-16	41	J3-14	
	D8	40	J3-4	65	J3-15	
	A7	63	J4-15	39	J3-16	
GND	G4	9	J4-34	3	J3-17	
	B4	49	J4-18	37	J3-18	
	F8	24	J3-33	5	J3-19	
	A8	64	J4-17	35	J3-20	
	H7	7	J4-31	7	J3-21	
	G8	16	J4-20	33	J3-22	
	G3	10	J4-32	9	J3-23	
	H4	1	J4-19	31	J3-24	
	H6	6	J4-29	11	J3-25	
	G7	15	J4-22	29	J3-26	
	G2	11	J4-30	13	J3-27	
	H3	2	J4-21	27	J3-28	
	H5	5	J4-27	15	J3-29	
	B5	53	J4-10	53	J3-3	
	G6	14	J4-24	25	J3-30	
	G1	12	J4-28	17	J3-31	
	H2	3	J4-23	23	J3-32	
	H1	4	J4-25	19	J3-33	
	G5	13	J4-26	21	J3-34	
	A1	60	J4-9	51	J3-4	
	A2	59	J4-7	55	J3-5	
	B1	52	J4-12	49	J3-6	
	B6	54	J4-8	57	J3-7	
	A5	61	J4-11	47	J3-8	
	A3	58	J4-5	59	J3-9	
	E6	30	J3-24	26	J4-10	
	E2	27	J3-30	14	J4-11	
	F3	18	J3-21	28	J4-12	
	F5	21	J3-27	16	J4-13	
	E7	31	J3-22	30	J4-14	
	E1	28	J3-28	18	J4-15	
	F4	17	J3-19	32	J4-16	
GND	B8	56	J4-4	36	J4-17	
	E8	32	J3-20	34	J4-18	
GND	H8	8	J4-33	68	J4-19	
	C8	48	J3-17	38	J4-20	
	C1	44	J3-9	54	J4-21	
	D4	33	J3-18	40	J4-22	
	D5	37	J3-10	56	J4-23	
	C7	47	J3-15	42	J4-24	
	C2	43	J3-7	58	J4-25	
	D3	34	J3-16	44	J4-26	
	D6	38	J3-8	60	J4-27	
	C6	46	J3-13	46	J4-28	
	C3	42	J3-5	62	J4-29	
	E4	25	J3-34	6	J4-3	
	D2	35	J3-14	48	J4-30	
	D7	39	J3-6	64	J4-31	
	C5	45	J3-11	50	J4-32	
	C4	41	J3-3	66	J4-33	
	D1	36	J3-12	52	J4-34	
	F1	20	J3-25	20	J4-4	

Pic. of modified 3-in-1 Brd

3 modified pins